ADVANCED ENERGY MATERIALS

Supporting Information

for *Adv. Energy Mater.,* DOI: 10.1002/aenm.202002129

The Electronic Structure of MAPI-Based Perovskite Solar Cells: Detailed Band Diagram Determination by Photoemission Spectroscopy Comparing Classical and Inverted Device Stacks

*Tim Hellmann, Chittaranjan Das, Tobias Abzieher, Jonas A. Schwenzer, Michael Wussler, Ralph Dachauer, Ulrich W. Paetzold, Wolfram Jaegermann, and Thomas Mayer**

Supporting Information

The Electronic Structure of MAPI based Perovskite Solar Cells: Detailed Band Diagram Determination by Photoemission Spectroscopy Comparing Classical and Inverted Device Stacks

Tim Hellmann[1], Chittaranjan Das[1], Tobias Abzieher[2], Jonas Schwenzer[2], Michael Wussler[1], Ralph Dachauer[1], Ulrich Wilhelm Paetzold[2,3], Wolfram Jaegermann[1], Thomas Mayer*[1]

[1]Surface Science Group, Materials Science Department, Technical University of Darmstadt, Alarich-Weiss-Straße 2, 64287 Darmstadt, Germany

[2]Light Technology Institute, Karlsruhe Technology Institute, Engesserstraße 13, 76131 Karlsruhe, Germany

[3]Institute of Microstructure Technology, Karlsruhe Institute of Technology, Hermann-von-Helmholtz-Platz 1, Germany

Corresponding author: Thomas Mayer (mayerth@surface.tu-darmstadt.de)

1. JV curves of a device in classical and inverted architecture

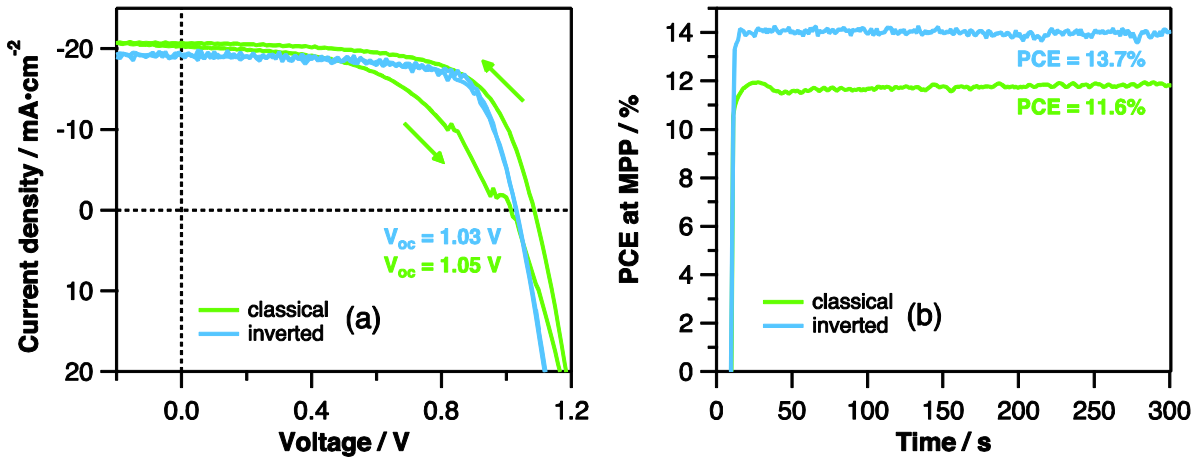

Figure S1: Typical JV-curves of a classical and an inverted device (left) and the PCE at the maximum power point (MPP) over 300 s (right).

2. UV/VIS and XRD measurements of MAPI films deposited on SnO_2 and NiO_x

Figure S2 (a) UV/Vis and (b) XRD measurements of vacuum deposited MAPI perovskite films on SnO_2 and NiO_x substrates. In Figure S2 (a) both films are showing a clear absorption edge at 780 nm, which fits to the band gap value of 1.58 eV reported for MAPI in literature. No indication of a PbI_2 absorption edge at 540 nm is given. In Figure S2 (b) the XRD measurements show a cubic perovskite phase for both substrates. Small diffraction peaks of PbI_2 are observed for MAPI on SnO_2 which are even smaller on NiO_x. Additional peaks from the underlying ITO substrates are visible as well. Interestingly the MAPI texture is different for the SnO_2 and NiO_x substrate, namely (100) on SnO_2 and (111) on NiO_x.

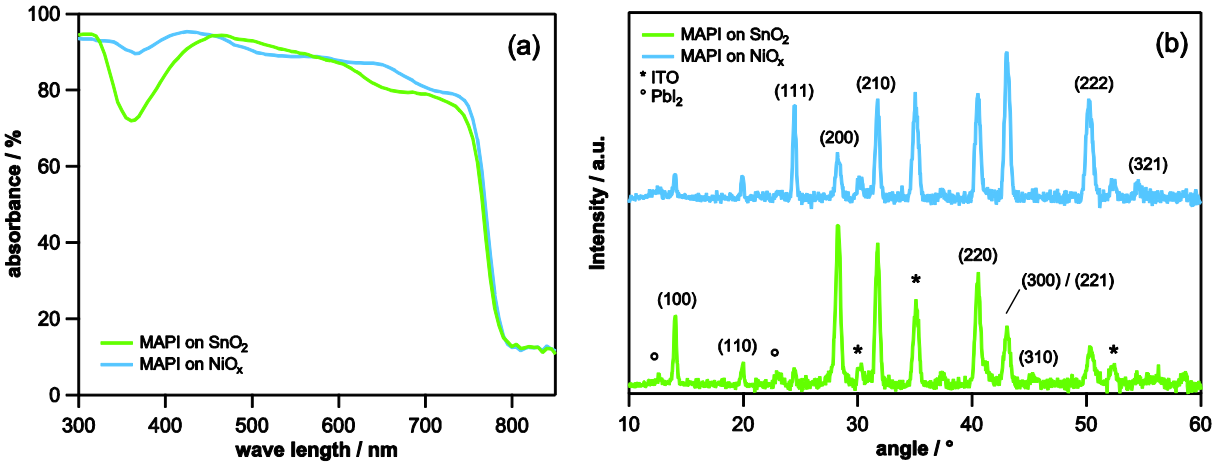

Figure S2: UV/Vis measurements (a) and XRD measurements (b) of a MAPI film deposited on SnO_2 and NiO_x.

3. Determination of the VBM of MAPI

Figure S3 (a), (b) and (c) are showing the $I3d_{5/2}$ emission line, the Pb4f emission line and the valence band region of the in-vacuo prepared reference sample. The $I3d_{5/2}$ and the $Pb4f_{7/2}$ emission line are positioned at 619.48 eV and 138.57 eV. A VBM of 1.38 eV is determined from the logarithmic plot. The corresponding core level to VBM distances are 618.10 eV for the $I3d_{5/2}$ and 137.19 eV for the $Pb4f_{7/2}$ emission line. These core level to VBM distances of the reference sample can now be used to predict the VBM of the two perovskite samples from the main article. The calculated values for the predicted VBM of the perovskite absorber on SnO_2 and NiO_x are 1.38 eV and 1.52 eV, which is comparable to the VBM values determined from fitting the valence band onset in the logarithmic plot (see Table S1). The authors want to emphasize that the main conclusion of this will work is not influenced by the way of determining the VBM. For both methods (VBM from linear and logarithmic plot) the perovskite absorber appears n-type and the band diagrams that are derived later in the article with the help of the perovskite VBM values will not be affected strongly.

Table S1: The core level positions, predicted VBM values from the core level to VBM distance of the reference sample and the VBM values determined from the logarithmic plot for the two perovskite samples that were used to construct the band diagrams for the main article.

MAPI Sample	$Pb4f_{7/2}$ / eV	$I3d_{5/2}$ / eV	predicted VBM / eV			VBM from log plot / eV
			from $Pb4f_{7/2}$	from $I3d_{5/2}$	average	
on SnO_2	138.56	619.50	1.37	1.40	1.38	1.35
on NiO_x	138.70	619.63	1.51	1.53	1.52	1.43

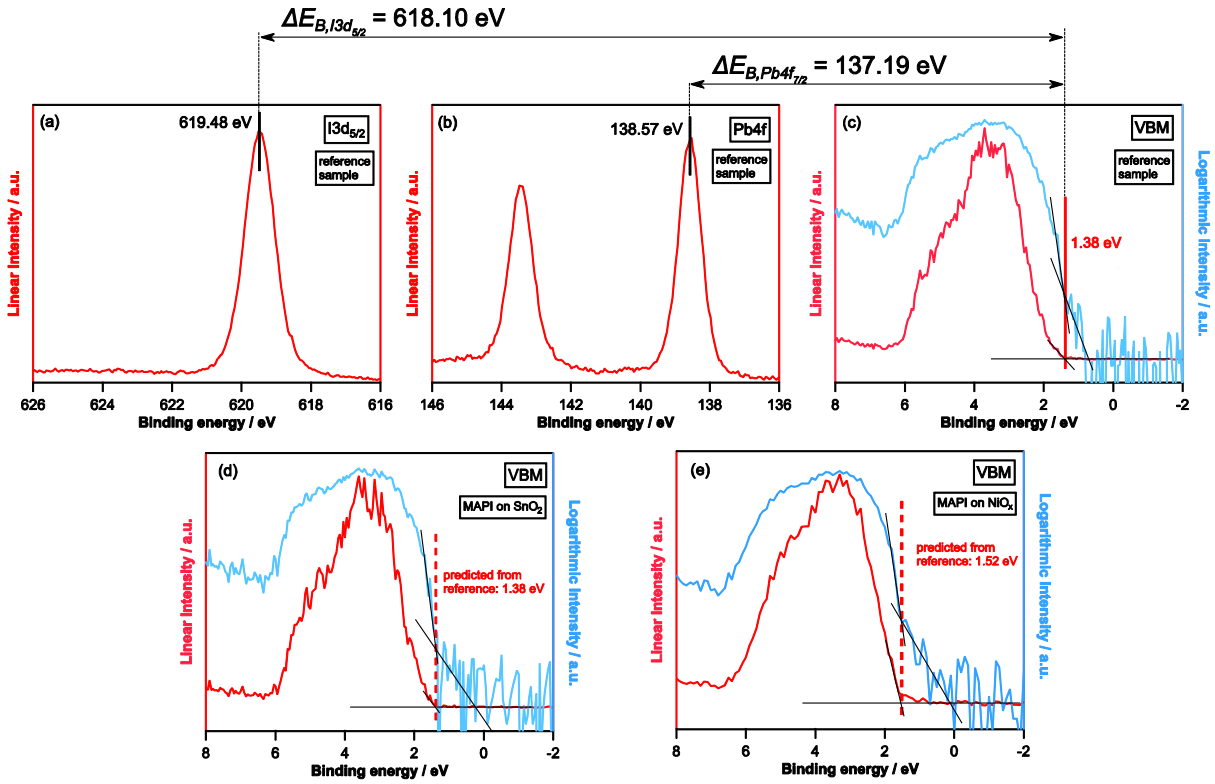

Figure S3: Detailed scans of the $I3d_{5/2}$ emission line (a), the Pb4f emission line (b) and the valence band region (c) of the reference sample and corresponding distances between the core levels and the VBM. (d) and (e) are showing the valence band regions for the two MAPI films deposited on SnO_2 and NiO_x from the main mansuscript.

4. He I measurements to determine work functions

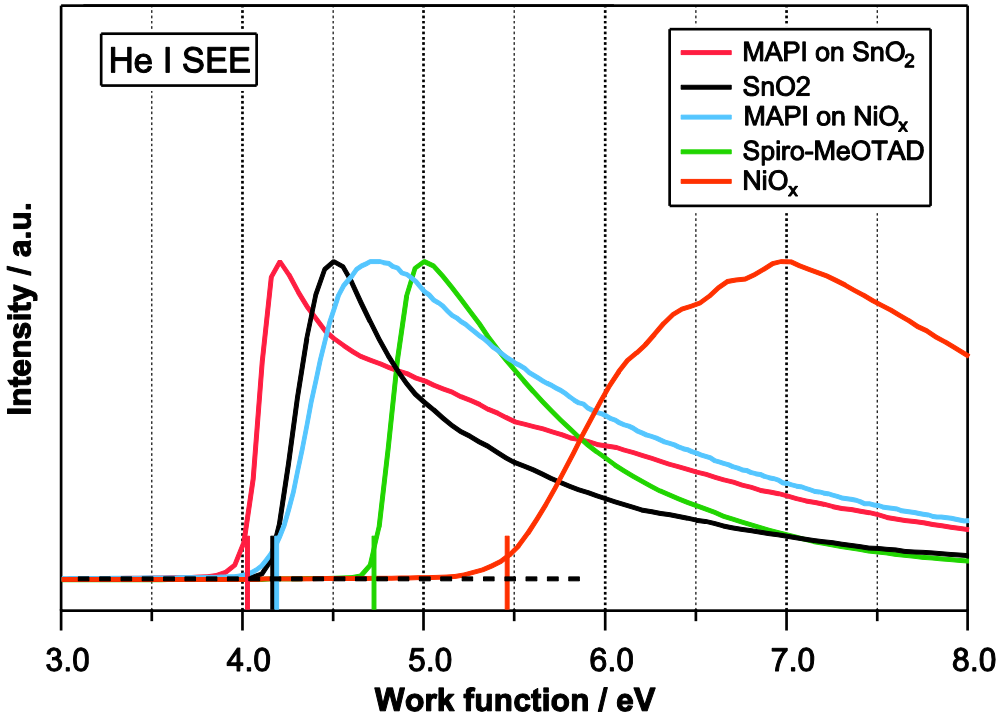

Figure S4: He I measurements of the secondary electron edge with an applied bias of – 6 V to determine the work function.

5. Dark / light measurements of different perovskites on SnO_2 and NiO_x substrates

Additional PES measurements in the dark and under illumination of FAPI, CsFAPI, MAFAPI and CsMAFAPI perovskites deposited by spin-coating on SnO_2 and NiO_x substrates are performed (see Figure S5). Like the results for MAPI presented in the main article (see Figure 2) the perovskites deposited on NiO_x show a binding energy shift to lower binding energies upon illumination, which indicates a positive surface photovoltage. For the perovskite on SnO_2 no such shift is observed. When used in devices, the FAPI, CsFAPI, MAFAPI and CsMAFAPI perovskite films can reach efficiencies of up to 16.4 %, 17.0 %, 19.2 % and 17.4 %, respectively.

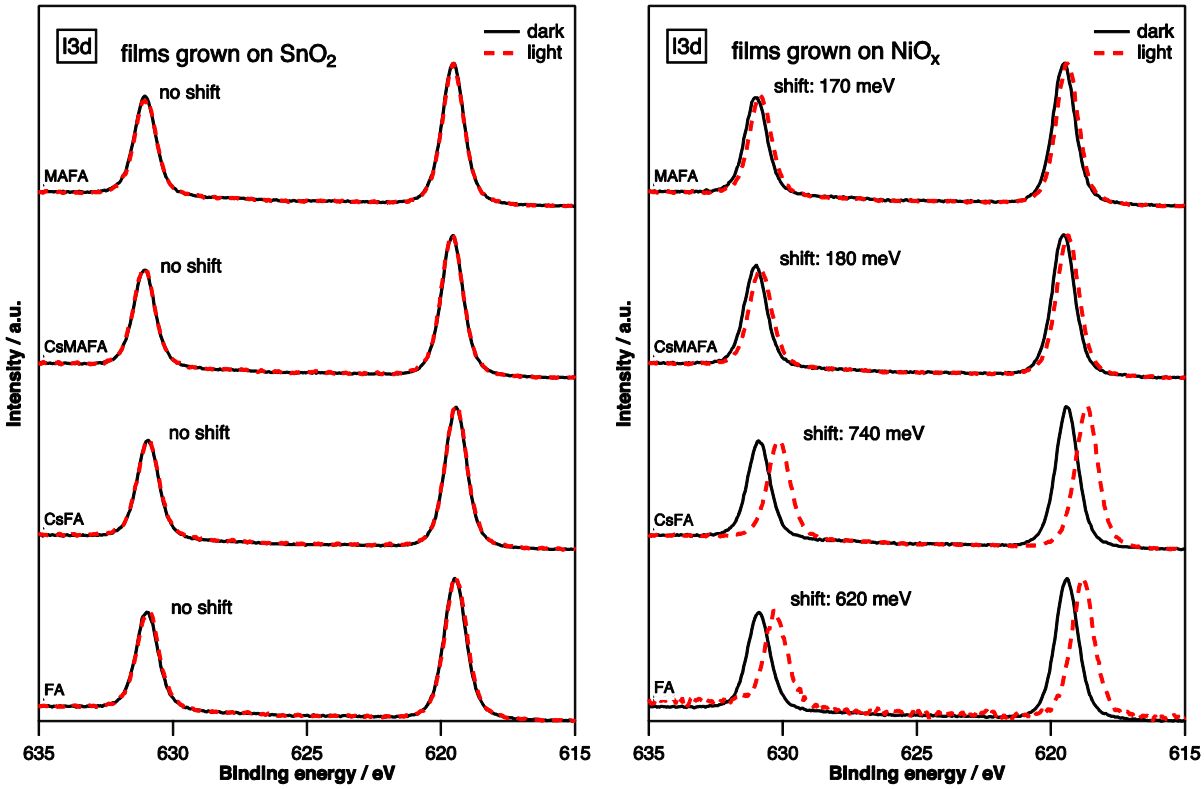

Figure S5: XPS measurements of the I3d emission line for four different perovskites deposited on SnO_2 (left) and NiO_x substrates (right). The samples were measured in the dark (solid black line) and under illumination (broken red line). For the perovskites on NiO_x the illumination results in a shift to lower binding energies, which indicates the presence of a surface photovoltage.

6. Detailed analysis of the NiO_x | MAPI interface

To provide evidence for the built-in potential at the NiO_x | MAPI interface, a detailed analysis of this interface is performed. Since a step-by-step deposition of MAPI in the nanometer range is experimentally quite challenging, a tapered cross section of the NiO_x | MAPI interface was prepared and measured. For this, a several hundred nanometer thick layer of the perovskite absorber is first deposited on a NiO_x substrate and then transferred into a small angle tapered edge by polishing the surface. This approach allows to extend the interface between NiO_x and MAPI from a few nanometers to a several millimeters, allowing to measure the interface by scanning the X-ray beam along the incline. A more detailed description of the sample preparation and the measurement of a full perovskite solar cell has been reported by the authors elsewhere.[1] Figure S6 (a), (b) and (c) show the detailed scans of the Pb4f, the I3d and Ni2p emission line of the tapered cross section. From bottom to top the sample is measured from the bare NiO_x surface along the interface towards the bulk of MAPI. The Ni2p emission line does not show any binding energy shift, indicating a flat band inside the NiO_x. The $Pb4f_{7/2}$ and $I3d_{5/2}$ emission lines are both shifting to higher binding energies by about 300 meV, which indicates a downward band bending inside the MAPI. The second $Pb4f_{7/2}$ at around 136.8 eV can be attributed to Pb(0), which is commonly observed for prolonged XPS measurements.

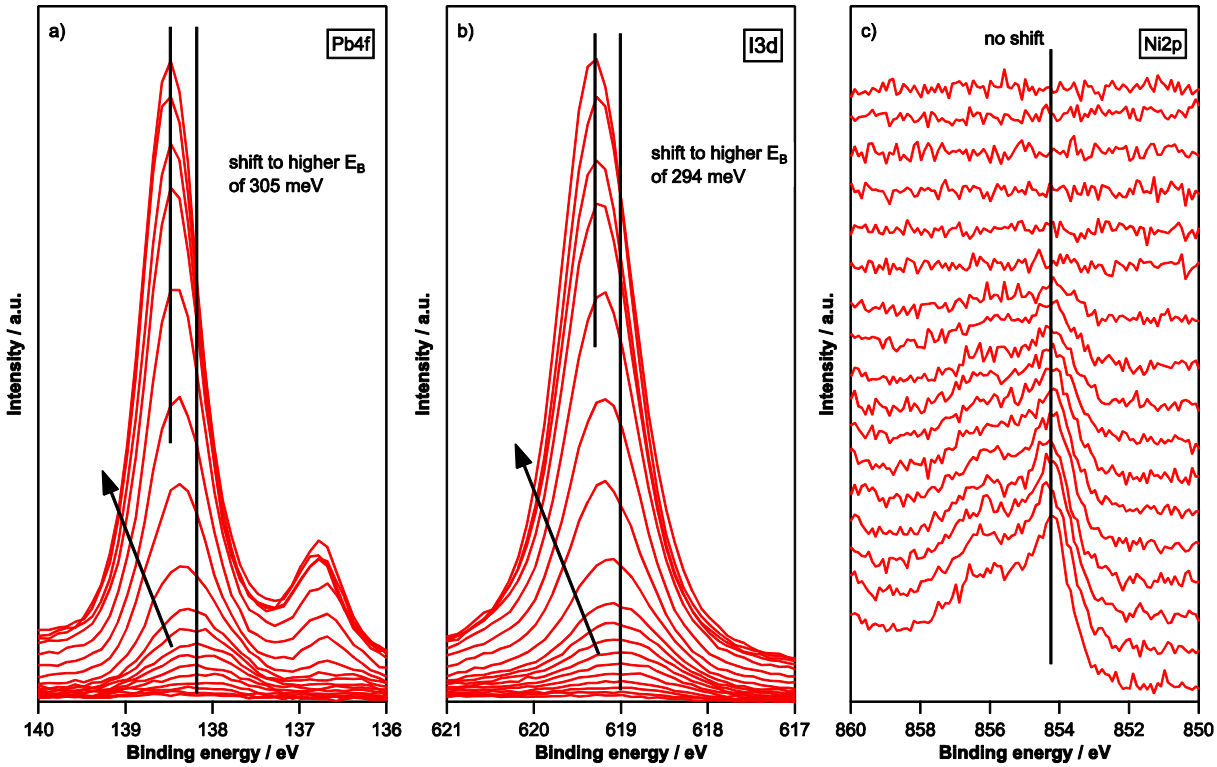

Figure S6: Detailed scans of the Pb4f emission line (a), the I3d emission line (b) and the Ni2p emission line (c) of the interface between NiO_x and MAPI. From bottom to top the MAPI thickness increases. The Ni2p emission show no binding energy shift, indicating that there is no band bending inside the NiO_x. The Pb4f and I3d emission lines show shifts to higher binding energies, indicating a downward band bending inside the MAPI perovskite towards its bulk.

7. Detailed analysis of the MAPI | spiro-MeOTAD:LiTFSI interface

The electronic structure at the interface between MAPI and LiTFSI doped spiro-MeOTAD is investigated by co-depositing spiro-MeOTAD and LiTFSI onto a MAPI substrate and performing XPS measurements in the dark and under illumination after each deposition step. Figure S7 (a) and (b) are showing the N1s and the C1s emission lines. For the N1s emission line of MAPI no binding energy shift is observed, indicating that there is no band bending present inside the perovskite absorber. The N1s emission of spiro-MeOTAD is shifting to lower binding energies, indicating a band bending downward towards the interface. For the C1s emission line, a binding energy shift to lower binding energies is observed as well. Upon illumination, the C1s emission line shifts to higher binding energies, the flat band is achieved for the respective spiro-MeOTAD thickness, due to the formation of a SPV.

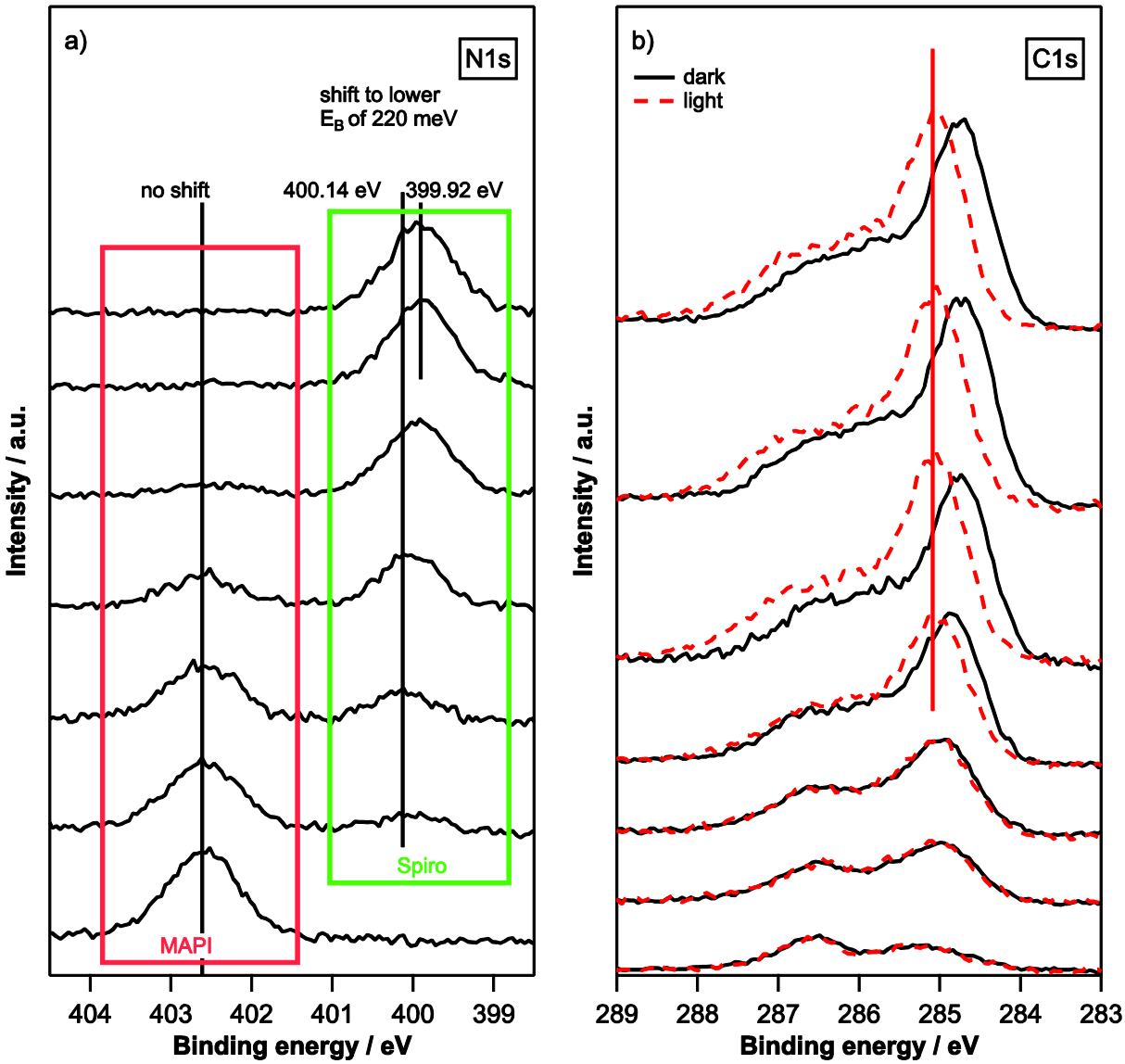

Figure S7: Detailed scans of the N1s emission line (a) and the C1s emission line (b) of the interface between MAPI and spiro-MeOTAD doped with LiTFSI. From bottom to top the spiro-MeOTAD:LiTFSI thickness increases. In the dark (black solid curves), the N1s emission line of MAPI does not show any binding energy shift, indicating a flat band inside the perovskite. The N1s emission line of Spiro-MeOTAD is shifting to lower binding energies, indicating an upward band bending inside the spiro-MeOTAD towards its bulk. In the C1s emission line the binding energy shift to lower binding energies is visible as well. Upon illumination (red broken curves), the band bending inside the Spiro-MeOTAD becomes flat and a SPV forms, which is visible by the shift of the C1s emission lines to higher binding energies.

8. Valence band measurements used to construct the band diagrams

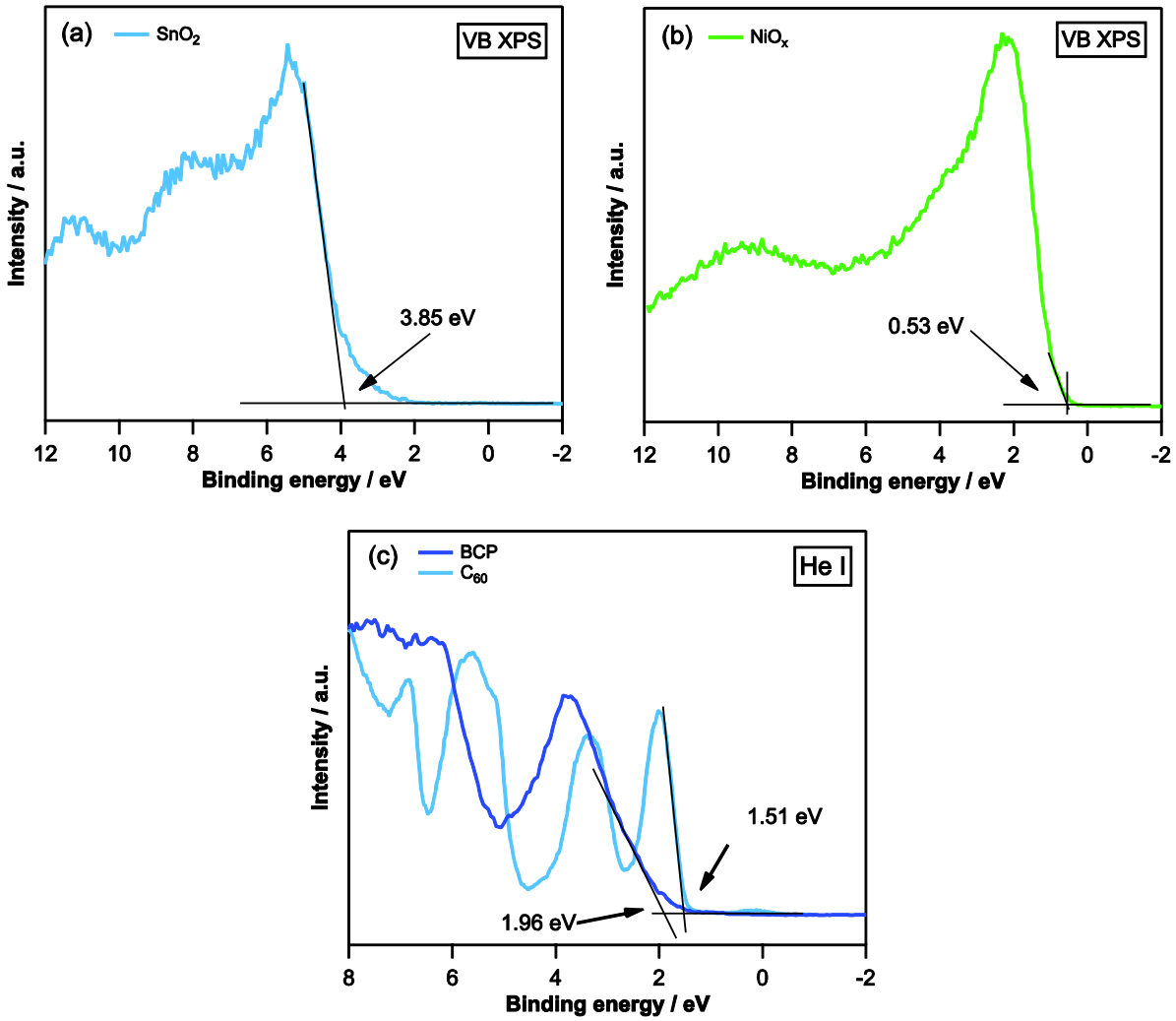

Figure S8: XPS and He I valence band measurements of a (a) SnO_2 surface, (b) NiO_x surface and of a (c) C_{60} and BCP surface to determine the valence band to Fermi level distances.

9. Detailed analysis of the MAPI | C_{60} interface

The electronic structure at the interface between MAPI and C_{60} is investigated in more detail by a stepwise deposition of C_{60} onto a MAPI surface. Figure S9 (a) and (b) are showing the I3d and the C1s emission lines for different C_{60} thickness. In both cases there is no binding energy shift visible, which indicates that there is no band bending present at the MAPI | C_{60} interface.

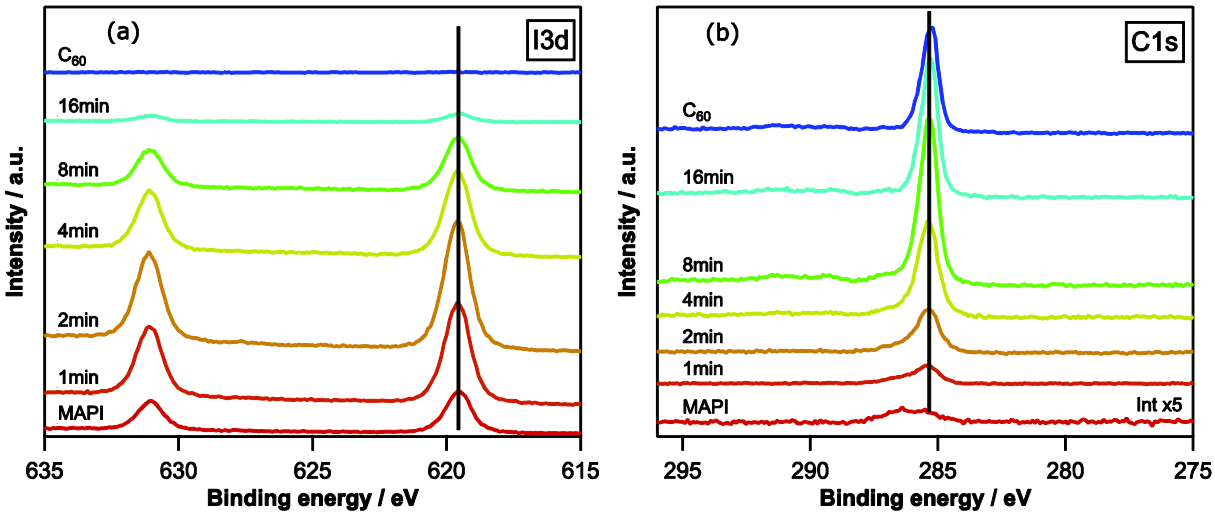

Figure S9: XPS measurements of the I3d emission lines for the MAPI | C_{60} interface. No binding shift indicates no band bending is present inside the perovskite absorber and the C_{60} layer.

10. Information about the lamp used to illuminate the sample during the PES measurements

For the light measurements, a 50 W ECONLUX SolarRaptor tungsten high-intensity discharge (HID)-lamp was attached to one of the glass view ports of the XPS measurement chamber and the sample was illuminated from a distance of roughly 50 cm at an angle of around 45°. To estimate the light intensity that reaches the perovskite absorber layer in the XPS chamber, a pyranometer was positioned inside a dark box in air at a similar angle and illuminated through an identical window at a distance of 50 cm. A power density of 1540 W/m² was determined. For a gold film with a thickness of 25 nm it is reported that around 25% of the light will be reflected at the Au | vacuum interface and around 55 % of the light will be absorbed inside the gold layer, which means that only around 11.25% of the original light intensity will reach the perovskite absorber (values for reflectance and absorption are for wavelengths of 492 nm, taken from).[2] Similar values of around 13% and 20% are reported for the transmittance of 33.0 nm and 11.5 nm thick gold film at wavelengths of 500 nm, respectively.[3] A rough estimate for the power density of the light reaching the perovskite absorber during the PES measurements under illumination is therefore around 200 W/m² (13% of the original measured 1540 W/m²), which is much lower than the power density used in the solar simulator measurements (1000 W/m² for AM1.5G). This lower power density is the reason why the observed photovoltages in the PES measurements are lower than the open-circuit voltages from the J-V-measurements using a solar simulator.

11. Calculation of the space charge region width

The width of the space charge region d_n can be calculated with the formula from Ibach[4] as given below, with ε being the permittivity, V_D the diffusion potential, N_A and N_D the acceptor and donor concentrations, ε_0 the vacuum permittivity and e the elemental charge.

$$d_n = \left(\frac{2 \cdot \varepsilon \cdot \varepsilon_0 \cdot V_D}{e} \cdot \frac{\frac{N_A}{N_D}}{N_A + N_D} \right)^{0.5}$$

This formula can be rewritten as:

$$d_n = \left(\frac{2 \cdot \varepsilon \cdot \varepsilon_0 \cdot V_D}{e} \cdot \frac{\cancel{N_A} \cdot \frac{1}{N_D}}{\cancel{N_A} \cdot (1 + \frac{N_D}{N_A})} \right)^{0.5}$$

If the space charge region only appears inside the MAPI perovskite (see Figure S6), it can be assumed that N_A is infinitely large, resulting in:

$$\lim_{N_A \to \infty} d_n = \left(\frac{2 \cdot \varepsilon \cdot \varepsilon_0 \cdot V_D}{e \cdot N_D} \right)^{0.5}$$

Bannow et al.[5] reported that the published values for the MAPI permittivity ε varies in the range of 20 to 70 (citing[6-9]) $V_D = 0.82\,V$ and $N_A = 2 \cdot 10^{20} cm^{-3}$, a space charge region width d_n of 3 to 5.6 nm results, which appears rather small.

12. Dependence of charge carrier concentration on Fermi level position:

The electron concentration is defined as[10]

$$n = N_C \cdot e^{-\frac{(E_C - E_F)}{k_B T}}$$

and can be expressed in dependence of the VBM as

$$n = N_C \cdot e^{-\frac{(E_g - E_{VBM})}{k_B T}}$$

showing that the Fermi level position in the energy gap (the VBM) enters exponentially into the electron concentration.

Literature

[1] M. Wussler, T. Mayer, C. Das, E. Mankel, T. Hellmann, C. Prawobo, I. Zimmermann, M. K. Nazeeruddin and W. Jaegermann, *Adv Funct Mater* **2020**, 1910679.

[2] O. Loebich, **1972**, *5*, 2-10.

[3] A. Axelevitch, B. Gorenstein and G. Golan, **2012**, *32*, 1-13.

[4] H. Ibach and H. Lüth, Solid-State Physics: An Introduction to Theory and Experiment Springer: 1981.

[5] L. C. Bannow, J. Hader, J. V. Moloney and S. W. Koch, *Apl Mater* **2019**, *7*.

[6] M. Sendner, P. K. Nayak, D. A. Egger, S. Beck, C. Muller, B. Epding, W. Kowalsky, L. Kronik, H. J. Snaith, A. Pucci and R. Lovrincic, *Mater Horizons* **2016**, *3*, 613-620.

[7] N. Onodayamamuro, T. Matsuo and H. Suga, *J Phys Chem Solids* **1992**, *53*, 935-939.

[8] Q. Q. Lin, A. Armin, R. C. R. Nagiri, P. L. Burn and P. Meredith, *Nat Photonics* **2015**, *9*, 106-112.

[9] F. Brivio, K. T. Butler, A. Walsh and M. van Schilfgaarde, *Phys Rev B* **2014**, *89*.

[10] A. Many, Y. Goldstein and N. B. Grover, Semiconductor Surfaces. North-Holland Pub. Co: 1965.